System-Wide Photocurrent Response in Gapless Materials

Justin C. W. Song[1,2] and Leonid S. Levitov[1]
[1] *Department of Physics, Massachusetts Institute of Technology, Cambridge, Massachusetts 02139, USA and*
[2] *School of Engineering and Applied Sciences, Harvard University, Cambridge, Massachusetts 02138, USA*

We develop a general Shockley-Ramo-type framework to describe spatial patterns of photocurrent response in gapless materials. Our approach helps to understand the striking features of the observed patterns, such as the directional effect and the global character of photoresponse. We illustrate this approach by examining specific examples, and show that the photoresponse patterns can serve as a powerful tool to extract information about symmetry breaking, inhomogeneity, chirality, and other local characteristics of the system. Short response times, originating from the nonlocality, make photocurrent uniquely sensitive to the charge and spin dynamics of the system.

The optoelectronic response of many gapped materials features spatial nonlocality arising due to slow recombination of photoexcited carriers[1]. Recently, scanning photoresponse techniques were used to probe new gapless materials, such as graphene and topological insulators, where carrier recombination is fast compared to the characteristic timescales for transport across the system (see Refs.[2–8] and references therein). Surprisingly, these studies revealed complex spatial patterns of photocurrent response. Rather than being localized near current-collecting contacts, the photocurrent hot spots are distributed over the entire system area, typically separated by many microns from the contacts [3–7]. These large length scales may seem hard to reconcile with the short picosecond-scale recombination times over which the photoexcited carriers lose their energy and become part of the thermal distribution, traversing distances much less than the system size.

Here, we introduce a framework that naturally explains how the non-locality can arise in the absence of slow recombination, and incorporates diverse local phenomena predicted theoretically[9–13]. Using this framework, we can understand striking features of the observed patterns [4–7], such as the global character of the response and the *directional effect* (Fig.1). Namely, the photocurrent hot spots are highly sensitive to the orientation of inhomogeneities and interfaces, at which the hot spots are pinned, but totally independent of the distance from the contacts [Fig.1(d) shows data from Ref.[4] where this effect was first reported]. Further, the resulting patterns are sensitive to the symmetries which govern photoresponse. This is illustrated for several mechanisms, charge-dominated (Fig.1) and spin-dominated (Fig.3). In the latter case, we show that the spatial pattern structure is directly sensitive to the details of spin dynamics.

In gapless materials, photoresponse is mediated by ambient carriers outside the photoexcitation spot. Short recombination times lead to a rapid decay of the primary photoexcited carriers, preventing them from reaching contacts and directly contributing to photocurrent. Instead, the main contribution is indirect: a local photocurrent sets up an e.m.f. that drives ambient carriers

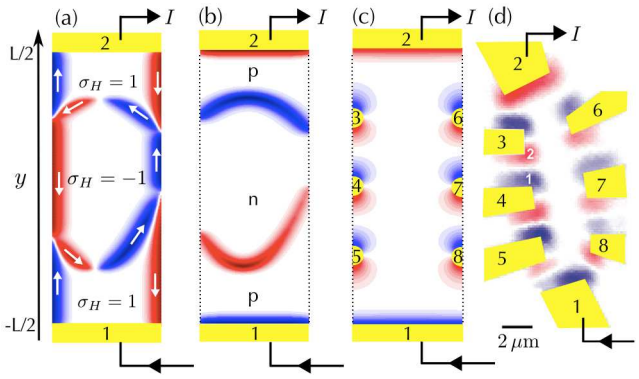

FIG. 1: Scanning photocurrent images for different mechanisms of photoresponse. The photocurrent, drawn from contacts 1 and 2, is modeled by Eqs.(1),(5). (a) Photocurrent pattern in a chiral material, where $\sigma_H = \pm 1$ marks regions of different chirality. Local photocurrent direction is governed by edge states (white arrows). (b) Photocurrent pattern in a non-chiral system with a step-like density inhomogeneity (see text). (c) Photocurrent pattern due to floating contacts that do not draw current (yellow semi-circles labeled 3-8). In all 3 cases, the system-wide photoresponse has strong directional dependence on the local photocurrent orientation and profile, but essentially no dependence on its location within the system. (d) Scanning photocurrent image of a 12 μm-long graphene device with six floating contacts 3-8. Note that the sign of photoresponse near floating contacts is correlated with the direction to the contacts 1 and 2 through which current is drawn (data taken from Fig.2(a) of Ref. [4]).

far from the excitation region, and into the contacts, leading to response which does not diminish with distance.

The "global" character of the response can be linked to charge continuity. The condition $\nabla \cdot \mathbf{j} = 0$ can be interpreted as incompressibility of current flow, with stream lines that do not terminate anywhere within the system. In addition, because the current is caused by a chemical potential gradient, the stream lines cannot close on itself. This results in a response at contacts far away from the spatial structures probed by the photoexcitation. As we shall see, the system-wide response to local photoexcitation can be described as

$$I = A \int \mathbf{j}_{\rm loc}(\mathbf{r}) \cdot \nabla \psi(\mathbf{r})\, d^2 r, \qquad (1)$$

where $\mathbf{j}_{\rm loc}(\mathbf{r})$ is local photocurrent in the photoexcitation region, ψ is a weighting field obtained by solving a suitable Laplace problem, and A is a prefactor which depends on device configuration (see Eq.(4)). Spatial patterns predicted using Eq.(1) exhibit photocurrent-active structures with contrast which is essentially independent on their position within the system (see Fig.1). Such "global" photoresponse is known for one-dimensional systems, where Eq.(1) reduces to adding up the total potential drop across the device [14]. However, the generalized framework presented here yields photocurrent that can exhibit complex structures which are not anticipated in a one-dimensional approach.

There is an interesting relation between our result and the seminal Shockley-Ramo (SR) theorem developed in the context of vacuum-tube electronics[15, 16]. Shockley and Ramo were concerned with the currents induced in the electrodes by charges moving in the free space inside the tube. The SR relation, which is intrinsically nonlocal due to the long range character of electric field in vacuum, can be expressed in a closed form as

$$I_{jk} \propto e\mathbf{v}(t)\cdot\mathbf{E}_w|_{\mathbf{r}=\mathbf{R}(t)}, \quad \mathbf{E}_w(\mathbf{r}) = \nabla w_{jk}(\mathbf{r}), \qquad (2)$$

where I_{jk} is the current induced by a moving charge e in the electrodes j and k, where $\mathbf{v}(t)$ and $\mathbf{R}(t)$ are the charge velocity and position. The function $w_{jk}(\mathbf{r})$ satisfies Laplace's equation with suitable boundary conditions on the electrodes. The SR theorem, which can be extended to charges moving in insulators[17], is key in ultra-fast charge sensing, such as particle detection in high energy physics[18, 19], plasma diagnostics[20], *etc.*

We emphasize that the origin of nonlocality in our photoresponse problem is quite different from that in the SR problem, since the ambient carriers screen the long range electric field created by photoexcited carriers. Instead, the nonlocality arises due to long range currents. Furthermore, the SR theorem is typically applied to high-speed charge detection, whereas we are concerned with the steady-state photocurrent. Yet, despite these differences, our approach yields a relation [Eq.(1)] which exhibits formal similarity with the SR theorem.

The starting point of our analysis is the continuity equation, $\nabla\cdot(\mathbf{j}_d+\mathbf{j}_{\rm loc})=0$, where $\mathbf{j}_d$ is the diffusion current due to ambient carriers in the material. These two contributions to current have very different spatial dependence: the photocurrent $\mathbf{j}_{\rm loc}$ is present in the excitation region, whereas the diffusion current $\mathbf{j}_d$ is nonzero throughout the entire material, describing the response to an e.m.f. due to $\mathbf{j}_{\rm loc}$ driving current far outside the excitation region. Below we focus on the simplest situation when transport can be described by a position-dependent conductivity tensor $\sigma(\mathbf{r})$ (other effects, such as the hot carrier transport [21, 22], can be analyzed similarly). The diffusion current satisfies the usual relation $\mathbf{j}_d = -\sigma(\mathbf{r})\nabla\phi$, where ϕ is the electrochemical potential. The boundary conditions in this transport problem are zero current through the sample boundary, $\mathbf{n}\cdot(\mathbf{j}_d+\mathbf{j}_{\rm loc})=0$, and constant potential at the contacts, $\mathbf{n}\times\nabla\phi=0$ (we assume a two-dimensional geometry).

To handle the non-local response, we introduce an auxiliary weighting field $\psi(\mathbf{r})$ satisfying $\nabla\cdot\mathbf{j}^{(\psi)}(\mathbf{r})=0$ in the bulk of the material, where $\mathbf{j}^{(\psi)}=-\sigma^{\rm T}\nabla\psi$, and appropriate boundary conditions at the boundary and contacts, $\mathbf{n}\cdot\mathbf{j}^{(\psi)}(\mathbf{r})=0$ and $\mathbf{n}\times\nabla\psi(\mathbf{r})=0$, respectively. Multiplying the continuity equation for the physical current $\mathbf{j}_d+\mathbf{j}_{\rm loc}$ by $\psi(\mathbf{r})$, integrating over the sample area, and using Gauss' theorem, we obtain

$$\int\nabla\psi(\mathbf{r})\cdot\mathbf{j}_{\rm loc}(\mathbf{r})d^2r = \sum_k \psi_k I_k - \phi_k I_k^{(\psi)} \qquad (3)$$

where k labels contacts. The quantities on the right hand side are the net currents flowing in each of the contacts, $I_k=\int_{C_k}\mathbf{n}\cdot\mathbf{j}_k d\ell$, and potentials on these contacts. We emphasize that Eq.(3) holds on very general grounds regardless of whether a particular contact is drawing current ($I_k\neq 0$) or is floating ($I_k=0$). The expression on the left hand side depends on the microscopic photocurrent distribution $\mathbf{j}_{\rm loc}(\mathbf{r})$ inside the material, whereas the expression on the right hand side is a function of currents and potentials at the contacts, thereby providing a general relation between position-dependent photoexcitation and the measured photocurrent.

It is convenient to choose $\psi(\mathbf{r})$ such that $I_k^{(\psi)}=0$ for all floating contacts. Then the contribution to Eq.(3) due to floating contacts drops out entirely, yielding a relation which only includes the contacts that actually draw current. It is also straightforward to account for the effect of an external circuit. We consider the current drawn through a pair of contacts 1 and 2 (see Fig.1) and write $I_{1(2)}^{(\psi)}=\mp(\psi_1-\psi_2)/R$, $I_{1(2)}=\pm(\phi_1-\phi_2)/R_{\rm ext}$, with R and $R_{\rm ext}$ the resistance of the sample and of the external circuit, respectively. Setting $\psi_1-\psi_2=1$, we obtain Eq.(1) with the prefactor

$$A = R/(R+R_{\rm ext}). \qquad (4)$$

Despite its apparent simplicity, Eq.(1) accounts for the key effects that impact photoresponse, such as system geometry, structure, inhomogeneity, chirality, etc.

The general features of Eq.(1) can be illustrated for a spatially uniform system of a rectangular shape. In this case, the weighting field $\psi(\mathbf{r})$ is a linear function, $\nabla\psi=\widehat{\mathbf{y}}/L$, with L the system length (see Fig.1). Constant $\nabla\psi$ leads to a "global" response which is invariant upon spatial translation of $\mathbf{j}_{\rm loc}(\mathbf{r})$. At the same time, the sign and the magnitude of the response depend on the angle between $\nabla\psi(\mathbf{r})$ and $\mathbf{j}_{\rm loc}(\mathbf{r})$ (the directional effect).

The value $\mathbf{j}_{\rm loc}(\mathbf{r})$ depends on system properties in the photoexcitation region. By symmetry, no photocurrent can occur in a spatially uniform system (assuming unpolarized light). In the presence of a density gradient

$\nabla n(\mathbf{r})$, the local photocurrent can be described by

$$\mathbf{j}_{\rm loc}(\mathbf{r}) = [\alpha \nabla n(\mathbf{r}) + \beta \widehat{\mathbf{z}} \times \nabla n(\mathbf{r})]\, J(\mathbf{r}), \qquad (5)$$

where α and β are material constants, and $J(\mathbf{r})$ is the absorbed optical power. In general, α is finite in all materials, whereas β is only non-zero in *chiral systems* where edge-state transport allows $\mathbf{j}_{\rm loc}$ to be directed along the contours of $n(\mathbf{r})$. This is the case in chiral materials such as topological insulators due to coupling between orbital motion and spin [8, 11, 12], or in non-chiral materials in the presence of a magnetic field[6].

The effects of spatial inhomogeneity are illustrated in Fig.1 for the chiral response (a) and the nonchiral response (b). For illustrative purposes, we use a step-like density profile, with n taking one value in the middle region and another value in the top and bottom regions, identical for (a) and (b). For (a) we use $\mathbf{j}_{\rm loc}$ with $\alpha = 0$ and finite β, for (b) it is the other way around. In both cases, the photocurrent is zero in the regions of constant n, and nonzero near the steps. The differences in the sign and magnitude of the response reflect the fundamental difference in physics in the cases (a) and (b).

Model (a) describes photoresponse in a chiral systems, which arises at the interfaces between domains of opposite chirality, labeled by $\sigma_H = \pm 1$. Physically, it may represent a quantum Hall system near a plateau transition[23], or a system in which nonzero chirality results from spontaneous ordering[24]. The different signs of chirality can be associated with the clockwise and counter-clockwise edge states, labeled by white arrows. Notably, the sign and magnitude of photocurrent depend on the direction of current flow in the edge states. The photocurrent is also nonzero at system boundaries, indicating the presence of current carrying edge states. This can be used to identify the edge states and domains with different chirality in experiment.

Fig.1 (b) shows the non-chiral photocurrent response for the same density profile as in Fig.1 (a). Physically, (b) may describe systems such as graphene with spatial inhomogeneity giving rise to p-n boundaries separating regions with electron-like and hole-like polarity [5]. In this case, $\mathbf{j}_{\rm loc}$ is normal to the contours of $n(\mathbf{r})$, making the sign and magnitude of the response dependent on the orientation of the interfaces viz. $\widehat{\mathbf{y}} \cdot \mathbf{j}_{\rm loc}$. Also, since $\mathbf{j}_{\rm loc}$ is normal to boundaries whereas $\nabla\psi$ is tangential, the photocurrent vanishes at the system edge.

A very different behavior is found near contacts, since $\nabla\psi$ is normal to the contact surface, see Fig.1 (c). In this case, a nonzero response arises both near the contacts through which current is drawn and near floating contacts (see also Fig.2). Notably, the response depends on the floating contact orientation but not on its position within the system. This is in agreement with experimental observations of Ref.[4], which are reproduced in Fig. 1 (d). All three photocurrent patterns in Fig.1, despite their different physical origin, share two common trends:

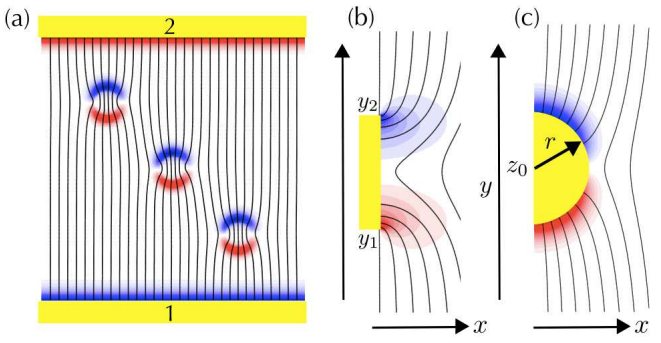

FIG. 2: Directional effect in photoresponse accounting fully for the distortions of the weighting field. (a) Photocurrent pattern due to three circular regions, modeled in the same way as in Fig.1 (b). The conductivity inside each region is taken to be 10 times larger than the background conductivity. (b,c) Photoresponse and the field lines for $\nabla\psi$ near floating contacts of two different shapes, a rectangle and a semicircle, obtained using the conformal mapping approach, Eq.(6).

strong directional sensitivity and global character (positional independence). This behavior makes the photocurrent patterns particularly useful in identifying symmetry breaking and inhomogeneity in gapless materials.

The patterns in Fig.1 (a),(b) were obtained using a spatially uniform weighting field approximation, $\nabla\psi \approx \widehat{\mathbf{y}}/L$. To analyze a more realistic inhomogeneous situation, we used a numerical procedure to obtain the exact profile $\psi(\mathbf{r})$. Fig.2 (a) shows photocurrent patterns from three circular regions with a mismatch between the inner and outer conductivity, which causes significant distortions of the $\nabla\psi$ field lines. Yet these distortions do not impact the overall trends discussed above, the global character of the response and the directional effect.

In contrast, the weighting field distortions have a very dramatic effect near contacts. Even if a contact does not draw net current, it *short-circuits* the current flowing in its vicinity, leading to a non-vanishing normal component of $\nabla\psi$ near the surface of a contact (see Fig. 2). For $\mathbf{j}_{\rm loc}$ which is normal to the contact, this gives a nonzero, sign-changing photoresponse, as in Fig.1 (c,d).

For ideal contacts, the field ψ can be found using the conformal mapping approach, giving $\psi(\mathbf{r}) = A\,{\rm Im}\, w(z)$. Here w is a suitable analytic function of a complex variable $z = x + iy$, which satisfies the equipotential condition at the contact surface. We illustrate this for a flat contact and for a semicircular contact (see Fig.2 (b,c)):

$$w_{\rm b}(z) = \sqrt{(z-y_1)(z-y_2)}, \quad w_{\rm c}(z) = z - z_0 - \frac{r^2}{z-z_0}, \qquad (6)$$

where the flat contact is positioned at $y_1 < y < y_2$, $x = 0$, and the semicircular contact is of radius r and is positioned at $z = z_0$. Here we assume that the contacts are floating and are small compared to the system size. At large z, ψ asymptotically approaches the linear dependence $\psi \propto y$ found above. The photocurrent at the

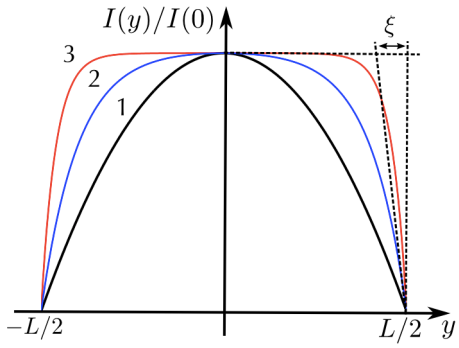

FIG. 3: Spatial dependence of spin-driven photocurrent, Eq.(9),(8), for spin diffusion length values $\xi = 5L$, $L/10$, $L/25$ (curves 1,2,3). Spin-diffusion length ξ can be directly determined from the measured photocurrent profile.

contact is proportional to $\mathbf{n}\cdot\nabla\psi$. For the flat contact,

$$\partial_x\psi(\mathbf{r})_{x=0} = A\frac{y-\frac{1}{2}(y_1+y_2)}{\sqrt{(y-y_1)(y_2-y)}}, \quad y_1 < y < y_2. \quad (7)$$

Since this quantity is an odd function of $y-\frac{1}{2}(y_1+y_2)$, the net current drawn the contact vanishes, as appropriate for a floating contact. Similar sign-changing behavior is found for the semicircular contact, see Fig.2 (c). The sign-changing pattern is oriented in such a way that the parts with high photoresponse are facing the contacts through which the photocurrent is drawn, in agreement with the observations reported in in Ref.[4], see Fig.1(d).

The approach described above can be applied to a variety of photocurrent mechanisms. As an illustration, we discuss the spin-driven photocurrent which arises in materials without inversion symmetry, in particular the topological insulators [8, 25, 26] and zinc-blende systems[27]. In such systems, spin orientation by circular polarized light results in spin imbalance $\mathbf{S}(\mathbf{r}) \propto J(\mathbf{r})$, generating local photocurrent via

$$\mathbf{j}_{\rm loc}(\mathbf{r}) = Q\mathbf{S}(\mathbf{r}). \quad (8)$$

Here Q is a second-rank tensor describing the spin-galvanic effect. Since the system-wide photoresponse, Eq.(1), is sensitive to spatial distribution of spin, it can be used to probe spin dynamics and relaxation.

As an illustration, we consider the rectangular geometry of Fig.1, and assume weak spin flip rate. In the diffusive limit, spin transport is governed by $-D\nabla^2\mathbf{S}+\mathbf{S}/\tau = J_{\mathbf{S}}$ [28], where $J_{\mathbf{S}}$ describes spin orientation by absorbed light. Evaluating the photocurrent, Eq.(1), we find

$$I(y)/I(0) = \left(\cosh\frac{L}{2\xi} - \cosh\frac{y}{\xi}\right) / \left(\cosh\frac{L}{2\xi} - 1\right) \quad (9)$$

where $\xi = \sqrt{D\tau}$. Notably, for $\xi \ll L$, the current is finite even when spins decay before reaching contacts. In contrast to the charge-dominated response, photocurrent vanishes near contacts which act as a spin sink. The measured profile $I(y)$ can be used to directly determine the spin diffusion length (see Fig.3).

Importantly, ambient carriers lead to a very fast photoresponse. A simple estimate of timescales can be given by reinstating the time dependent term in the continuity equation. For a spatially uniform system, the dynamics can be expressed in terms of the Fourier harmonics of charge density, $\partial_t\delta n_{\mathbf{k}}(t) = -\frac{2\pi}{\kappa}\sigma|\mathbf{k}|\delta n_{\mathbf{k}}(t)$, where σ is the sheet conductivity per square area and κ is the dielectric constant. For a crude estimate, taking parameter values $|\mathbf{k}| \approx \pi/L$, $L = 10\,\mu$m, $\kappa = 5$, $1/\sigma = 1\,$kΩ, we obtain a sub-picosecond response time

$$\tau = \kappa L/(2\pi^2\sigma) \approx 0.3\,\text{ps}, \quad (10)$$

which is considerably shorter than typical cooling and recombination times. Fast response makes the system-wide photocurrent a useful probe for the dynamical processes in the excitation region. It also makes gapless materials viable for applications in high-speed optoelectronics.

In summary, our approach explains several puzzling aspects of photocurrent response in gapless materials, in particular the striking non-locality and the *directional effect* observed in Ref.[4]. By analyzing different mechanisms of photoresponse, we demonstrate that it is uniquely capable of revealing spatial patterns arising due to symmetry breaking, chirality, or inhomogeneities. Sub-picosecond response times make photoresponse a useful probe of system dynamics.

We acknowledge useful discussions with M. Rudner and X. Xu, and financial support from the NSS program, Singapore (JS) and the Office of Naval Research Grant No. N00014-09-1-0724 (LL).

[1] S. M. Sze, K. K. Ng, *Physics of Semiconductor Devices*, 3rd Edition, Wiley, New York (2007).
[2] F. Bonaccorso, Z. Sun, T. Hasan, and A.C. Ferrari, Nat. Photonics **4** 611 (2010).
[3] F. Xia *et al.*, NanoLett. **9**, 1039 (2009)
[4] J. Park, Y. Ahn, C. Ruiz-vargas, NanoLett. **9** 1742 (2009)
[5] M. C. Lemme *et al.*, NanoLett. **11**, 4134-4137 (2011)
[6] G. Nazin, Y. Zhang, L. Zhang, E. Sutter, and P. Sutter, Nat. Phys., **6**, 870 (2010).
[7] R. Roy, M. Li, G. Aivazian, W. Yao, D. Cobden, C. Zhang, X. Xu, unpublished.
[8] J. W. McIver *et al.*, Nat. Nano, 10.1038/nnano.2011.214 (2011).
[9] P. Kral, E. J. Mele, D. Tomanek, Phys. Rev. Lett. 85, 15121515 (2000)
[10] E. Deyo, L. E. Golub, E. L. Ivchenko, B. Spivak, arXiv:0904.1917
[11] J. E. Moore, and J. Orenstein, Phys. Rev. Lett., **105**, 026805 (2010).
[12] P. Hosur, Phys. Rev. B, **83**, 035309 (2011).
[13] F. Rana *et al.*, Phys. Rev. B 79, 115447 (2009)
[14] J. Nelson, *The Physics of Solar Cells*, Imperial College Press, London (2003).
[15] W. Shockley, J. App. Phys. **9**, 635 (1938).
[16] S. Ramo, Proc. IRE, **27**, 584 (1939).

[17] G. Cavalleri, E. Gatti, G. Fabri, and V. Svelto, Nuc. Inst. Meth., **92** 137 (1971).
[18] P. D. Yoder, K. Gärtner, and W. Fichtner, J. App. Phys., **79** 1952 (1996).
[19] Z. He, Nuc. Inst. Meth. Phys. Res. A, **463**, 250 (2001).
[20] G. Maero, B. Paroli, R. Pozzoli, and M. Romé, Phys. Plasmas, **18**, 032101 (2011).
[21] N. M. Gabor, *et. al.*, Science, **334**, 648 (2011).
[22] J. C. W. Song *et. al.*, NanoLett., **11**, 4688 (2011).
[23] D. B. Chklovskii, B. I. Shklovskii, and L. I. Glazman, Phys. Rev. B, **83** 035309 (1992).
[24] R. Jamei, S. Kivelson, and B. Spivak, Phys. Rev. Lett., **94**, 056805 (2005).
[25] D. Hsieh, *et. al.*, Science, **323**, 4196 (2009).
[26] H. Hasan, C. L. Kane, Rev. Mod. Phys., **82**, 3045 (2010).
[27] S. D. Ganichev, *et. al.*, Nature, **417**, 513 (2002).
[28] A. A. Burkov, A. S. Nunez, and A. H. MacDonald, Phys. Rev. B, **70** 155308 (2004).